A comparative study of the mechanical and tribological properties of PECVD single layer and compositionally graded TiSiCN coatings

Mohammad Abedi[1], Amir Abdollah-zadeh[*,1], Antonello Vicenzo[2], Massimiliano Bestetti[2], Farid Movassagh-Alanagh[1], Elyad Damerchi[1]

[1]*Department of Materials Eng., Tarbiat Modares University, P.O. Box 14115-143, Tehran, Iran*

[2] *Department of Chemistry, Materials and Chemical Engineering "Giulio Natta", Politecnico di Milano, 20131 Milano, Italy*

Abstract

In this study, TiSiCN coatings, with and without a Ti/TiN/TiCN interlayer, are deposited on tempered and plasma-nitrided H13 hot-working tool steel substrate by pulsed direct current plasma enhanced chemical vapor deposition. The self-lubricant super hard TiSiCN coatings have a nanocomposite structure consisting of an amorphous SiCN matrix embedding TiCN nanocrystals. In the presence of the graded interlayer, coating adhesion improves significantly, as revealed by a 40% increase of the critical load for adhesion failure in scratch testing of the coated samples. The formation of shorter radial cracks around the indentation zone during Rockwell C indentation test reveals that the coating with the graded interlayer has a higher toughness compared to the single layer coating. The wear rate of the graded coating is found to be about three times lower than that of the single layer coating, which can

[*]Mail of corresponding author: zadeh@modares.ac.ir

Tel&Fax:+982182885040

be attributed to the higher hardness, better adhesion to the substrate and higher toughness of the graded coating.

Keywords: Nanocomposite coating, Superhard coating, Chemical vapor deposition, Graded structure.

1. Introduction

Hard and superhard coatings, with hardness in excess of 40 MPa, high toughness and superior thermal stability [1, 2], have raised great interest in the industry as high performance coating materials for a range of different uses, such as cutting tools, molding dies, mill components, and more generally mechanical parts for severe wear applications [3].

Among this class of coating materials, nanocomposite coatings of the TiSiN [3-6] and TiSiCN [3, 4, 7-10] families have received a greater attention during the last two decades. Industrial research is focusing on TiSiCN coatings for their versatility in both processing and use, addressing diverse demanding applications, as recent work suggests, such as high speed machining in dry or near-dry conditions [4] coating of piston rings [11], and of prosthesis components [12]. The availability of different processes for the deposition of TiSiCN coatings –namely Chemical Vapor Deposition, CVD [6-7], Plasma Enhanced (PE) CVD [5-8], sputtering [13] and plasma enhanced sputtering arc ion plating [14] has been influential to its industrial implementation by enabling processing in a wide range of conditions and tailoring of material properties. The microstructure of this coating –formed through self-organization as a result of spinodal transformation– consists of an amorphous matrix of silicon nitride or silicon carbonitride with a dispersion of TiCN nanocrystals [4, 7, 9]. A key property of this nanocomposite structure is the high thermal stability enabling TiSiCN coatings to maintain a high hardness up to 700 °C [8]. Additionally, if the carbon content in

TiSiCN is higher than the amount that can react with the other elements, the excessive carbon precipitates as amorphous carbon or diamond-like carbon (DLC) nanoparticles. The presence of self-lubricating nanoparticles in the microstructure of superhard TiSiCN coatings can significantly reduce its coefficient of friction (COF) [9]. Thanks to the combination of low COF and high hardness, TiSiCN coatings can provide excellent wear resistant compared to conventional nitride or carbo-nitride coatings [10].

Besides hardness and COF, adhesion to the substrate is another important property, which affects the durability of the coating significantly. The difference in stiffness and hardness between a hard thin coating and a soft substrate causes the substrate to experience a fraction of the force applied to the component; hence, the stress induced in the coating may be high enough to result in the fracture of the hard coating [15]. For instance, the elastic modulus and hardness of H13 hot-working tool steel are 210 GPa [16] and 6 GPa [17, 18], respectively; while, TiSiCN hard coatings have a modulus of elasticity of 300 GPa and hardness higher than 40 GPa [9, 10, 19]. Such large differences between the elastic modulus and hardness of the coating and those of the substrate can reduce the lifetime of the coated tools remarkably, and should be lowered in order to preserve coating integrity and adhesion [17]. The formation of a functionally graded interface underneath the hard coating via plasma nitriding of the steel substrate is a convenient and effective solution to this issue [20]. Typically, plasma nitriding can increase the surface hardness of H13 steel up to 10 GPa [17]. Another method used to improve the adhesion of a hard coating to a metallic substrate is the application of an interlayer. This method has been widely exploited over the last two decades and applied to hard coatings, such as amorphous carbon thin films on steel, e.g. [21, 22]. The interlayer should have good adhesion to both substrate and coating, while having hardness and elastic modulus intermediate between those of the coating and the substrate. It has been shown that functionally graded coatings are such an ideal interlayer thanks to through thickness

modulation of the mechanical properties achievable with an appropriate design of the layer stack [23]. The effective implementation of the above mentioned solutions –namely the formation of a functionally graded interface, the deposition of interlayers, or the deposition of functionally graded coatings– has been proven by a number of research studies, using different substrate and coating materials, e.g. [24-26].

In industrial applications, nitride coatings are conventionally synthesized using either CVD or physical vapor deposition (PVD) methods [27]. CVD processes require high deposition temperatures (800-900 °C), which are obviously too high for tool steels. Unlike CVD, PVD processes can be performed at low deposition temperature (200-300 °C); however, due to the physical nature of the process and the relatively low temperature, the formation of a high strength interface between coating and substrate is not easily attainable [27-29]. Therefore, PECVD was introduced as an appropriate method for depositing coatings at relatively low temperature, compared to CVD, preserving, at least to some extent, key advantages of CVD processes, such as good adhesion and conformal growth. In this method, the plasma discharge is used to provide the energy required for breaking down chemical bonds in the gas phase. In this way, the deposition temperature can be reduced significantly and steel substrates can be coated avoiding thermal damages. Also, using this method complex geometries can be coated uniformly, which may be difficult by PVD [29, 30].

In the current study, in order to increase the adhesion of TiSiCN nanocomposite coating deposited by PECVD on ASTM H13 hot-working tool steel, we use a functionally graded Ti/TiN/TiCN interlayer and investigate its effects on the structural and mechanical properties of TiSiCN coatings. To this purpose, TiSiCN coatings are deposited on plasma nitrided H13 hot-working tool steel with and without a functionally graded Ti/TiN/TiCN interlayer. The physicochemical, morphological and mechanical properties of the coatings are studied in details.

2. Experimental procedures

2.1. Specimen preparation

Prior to deposition, the H13 substrates were annealed at 1050 °C and quenched in oil. After quenching, the specimens were tempered at 550 °C for 1 h and cooled in air. After tempering, samples were first polished to a mirror finish, in order to remove the decarburized layer, then subjected to plasma nitriding to increase the surface hardness. The conditions of the plasma nitriding process are summarized in Table 1. TiSiCN coatings were deposited on two different sets of samples. The first set was held in the furnace for 3 h to obtain a single layer TiSiCN coating. The second set was first coated with a titanium layer by introducing hydrogen, argon and $TiCl_4$ vapor into the furnace. Then nitrogen was injected into the furnace increasing the flow rate by 1 sccm/min up to the constant level of 30 sccm. Similarly, the addition of methane was performed increasing the flow rate by 0.33 sccm/min up to the final constant value of 10 sccm. Finally, $SiCl_4$ vapor was supplied to the furnace, after which the deposition process continued for 3 h, according to Table 1. All deposition and plasma nitriding processes were carried out in a pulsed direct current plasma enhanced chemical vapor deposition (pulsed-DC PECVD) apparatus manufactured by Plasma Fanavar Amin (PFA) Company. Heating of the substrates was achieved through the plasma and a separate heater. The substrate temperature was measured by a thermocouple. After the deposition process, the samples were cooled in the furnace at low pressure to yield the structure schematically shown in Fig. 1.

2.2. Characterization

Glow discharge optical emission spectroscopy (GD-OES, Spectruma GDA750) analysis was used to determine the composition profile through the thickness of the coatings. The diffusion

depth of the plasma nitriding treatment of the H13 steel substrate was evaluated by hardness measurements using a microhardness testing machine (Asus, H13) equipped with a Vickers indenter. Field-emission scanning electron microscopy (FE-SEM) was used to study the nitride surfaces as well as the fracture surface of the coatings. The microstructure of the coatings was examined by a transmission electron microscope (TEM, Phillips CM200 FEG-TEM) at an operating voltage of 200 kV. The hardness and elastic modulus of the coatings were determined by a nanoindentation system (CSM nano/micro hardness tester) with a Berkovich tip under a maximum load of 50 mN. The adhesion strength of the coatings was assessed through two methods. In the first method, the micro-scratch test (CSM micro-scratch tester) was performed using a Rockwell C diamond indenter with a radius of 10 μm. However, the scratch test did not provide clear evidence of adhesion failure of the coatings, as noted further on. The second method for the evaluation of adhesion strength was based on VDI 3198 standard procedure. According to this standard, a Rockwell C indenter with a load of 150 kg is applied to the surface of coatings. Then, using optical microscopy (OM, Olympus), the adhesion strength of the coatings is evaluated by comparing the imprints images with the adhesion strength quality maps of the standard [31]. The surface roughness of coated samples was evaluated using the confocal microscope module integrated with the CSM micro-scratch test equipment. The wear resistance of the specimens was determined by a pin-on-disc test apparatus with a normal load of 5 N at a sliding speed of 5 m/min. The pin was made of 52100 steel and had a radius of curvature and hardness of 10 mm and 64 HRC, respectively. The wear tracks were examined by SEM and profilometry (Kosaka Surfcoder ET200).

3. Results and discussion

3.1. Microstructure

The surface of the steel substrate after the nitriding process is shown in Fig. 2. The nitrided layer shows a uniform granular morphology, which imparts a fine scale roughness to the surface, thus increasing the surface area and setting the conditions for a significant enhancement of the coating to substrate adhesion strength.

Fig. 3 shows the hardness depth profile across the nitrided layer. As expected, the hardness has a very high value at the surface, or zero depth, and shows a steep decrease with depth down to the hardness value characteristic of the substrate, at about 150 µm depth. Fig. 4 shows the SEM images of the cross-section of the coatings, with (Fig. 4 (b)) and without (Fig. 4 (a)) the Ti/TiN/TiCN interlayer. As can be seen, the thickness of the TiSiCN film is of about 2 µm for both samples, without and with interlayer. Apparently, for the latter sample, the graded composition layer at the interface with the substrate adds up to the overall thickness of the layer about 0.5 µm. We then used GDOES analysis to characterize the through thickness composition of the coatings. Fig. 5 shows the GDOES depth profile analysis of the TiSiCN coatings with and without the graded interlayer. Apparently, in either case, the TiSiCN layer has almost the same composition. For the coating without graded interlayer (Fig. 5 (a)), the GDOES profile confirms the thickness of about 2 µm, as revealed by SEM examination of the cross section. In addition, the depth profile analysis shows that the change in composition across the interface with the steel substrate occurs over the distance of about 500 nm. The main reason for this gradual change in the composition is the rough surface of the nitrided layer, which allows for the apparent formation of a diffuse interface. A peak in the titanium content can be seen at 2500 nm depth in the plot of Fig. 5 (a), which can be related to the accumulation of $TiCl_4$ vapor due to the rising temperature of the evaporator, prior to opening the drain valve for injection into the reaction chamber. Nevertheless, it is clear that the variation in the composition corresponding to this peak is relatively small compared to the change of the titanium content across the interface for the

graded coating, Fig. 5 (b). The GDOES depth profile for the latter sample shows that the composition of the coating is approximately constant to a depth of about 2 μm from the surface, while at higher depth there appears a steep increase of the titanium content and the attendant reduction in the content of the other components, in particular silicon. As already noted above, the depth resolution of the analysis is poor due to the high surface roughness of the substrate; consequently, profile broadening across the interface region does not allow to clearly resolve the composition depth profile of the interlayer.

TEM micrographs of the TiSiCN coatings shown in Fig. 6 reveals that the microstructure of both samples consist of nanocrystals embedded in an amorphous matrix. The nanocrystals, with size in the range of 10-60 nm, are almost uniformly distributed in the amorphous matrix. According to the results of selected area electron diffraction (SAED) analysis, in the insets of Fig. 6, these are nanocrystals of TiCN. Since GDOES results indicate significant amount of silicon in the structure, it can be concluded that silicon is present in the amorphous phase as silicon nitride or silicon carbo-nitride phases.

3.2. Mechanical properties

Fig. 7 shows the diagrams of the COF and the corresponding intensity of the acoustic emission and OM images of the scratches versus the normal load, from the microscratch testing of single layer and graded TiSiCN coatings performed with the diamond indenter of 10 μm tip radius. Sudden jumps in the COF and acoustic emission are indications of change in the wear behavior of the coating. As shown by the OM images of the scratches, the first jump (L_{c1}) corresponds to the appearance of cracks in the coating and the second one (L_{c2}) may be attributed to edge chipping of the coatings, notably with the single layer sample showing removal of larger coating fragments. However, coating spallation was not observed even when performing the tests at the maximum load value of 30 N. According to Table 2,

there is no significant difference between hardness and elastic modulus of the samples. This can be related to the fact that at a depth of 2 μm from the surface, chemical composition and structure of both types of coatings are almost the same. Overall, the presence of the interlayer leads to the increase of the critical force (L_{c1}) for crack initiation, which demonstrates the higher toughness of the coating with the graded interlayer. Moreover, the TiSiCN coating without interlayer undergoes significant damage at the normal applied load of 2.7 N (L_{c2}); while a normal load of 3.8 N (L_{c2}) is required for initial chipping failure of the graded interlayer TiSiCN coating. This may be an indication of the positive effect of the graded interlayer also on improving the adhesion of TiSiCN coating to the steel substrate. For both samples, COF increases with increasing the normal force; however, COF of the coating without interlayer is generally lower than that of the coating with interlayer.

Further evidence in support of the above interpratation was sought for by performing SEM examination of samples after scratch testing, as shown in Fig. 8 (images were taken at a 45° tilt in order to provide a clearer view of the fracture surfaces). Sliding of diamond indenter on the surface causes plastic deformation in the substrate and consequently delamination of the coating near the scratch zone. The fracture surface and substrate surface of the coating without interlayer is smooth, while the coating with interlayer has a rough fracture surface and the substrate surface is also uneven. The smooth fracture surface of the TiSiCN coating without interlayer is an indication of its brittle fracture compared to the one with the interlayer. By improving the adhesion of the coating, it is expected that the delamination of the coating causes ploughing of the substrate or creates a more intense plastic deformation zone on the substrate. Hence, the smooth separation interface (substrate surface in Fig. 8) observed for the coating without interlayer points to a lower adhesion strength in comparison with the coating with interlayer.

Fig. 9 shows the OM images of the indentation made by Rockwell C indenter. In the Rockwell hardness test, the applied load causes the indenter to penetrate both the coating and the substrate. As the indenter penetration induces plastic deformation of the substrate in the contact area, the coating cracks near the indentation zone because it is unable to accommodate deformation. Moreover, since coating delamination is not observed in both samples, we conclude that both coatings have acceptable adhesion according to VDI3198 standard [31]. On the other hand, it is worth noting that specimens with and without interlayer are different in terms of size and number of cracks. The specimen without interlayer has fewer cracks; however, the crack length is larger than that of the specimen with interlayer. In the specimen without interlayer, circumferential cracks are also observed between radial cracks; while, the one with interlayer shows only radial cracks. Since applied load and substrate material are the same, the penetration depth (larger than the coating thickness) is similar for both samples and it can be assumed that the substrate experiences the same amount of plastic deformation. Then, the coatings crack near the interface to release the stress exerted by the indenter, but owing to better adhesion and higher toughness, the crack growth rate in the sample with interlayer is lower than that of the sample without interlayer. Conversely, in order to release the applied stress, a larger number of cracks must be formed in the coating with interlayer. This crack propagation arresting mechanism has an important effect in improving the performance of the coatings, implying that higher stress will be required for cracks to propagate.

In order to asses the wear properties of the coatings, pin-on-disk tests were performed and the obtained COF curves are shown in Fig. 10. The variation of COF with sliding distance is different for the two samples, with and without interlayer. For the single layer TiSiCN coating, the COF is in the range of 0.1 to 0.25 over the sliding distance of about 500 m. Beyond this limit, the COF shows a steady increasing trend, reaching a value higher than 0.3

at a sliding distance of about 650 m and even higher values at longer sliding distances. Conversely, the COF of the TiSiCN coating with interlayer shows a slightly decreasing trend up to the sliding distance of about 500 m. With increasing sliding distance, a blurred step appears in the curve over the range from about 500 to 600 m, which results in the increase of the COF to about 0.4 at a sliding distance of about 950 m.

The wear tracks of both samples were investigated using SEM and surface profilometry methods. As can be seen, the wear track of the single layer coating is wider and also deeper than that of the graded coating. The depth of the wear track of the single layer coating is about 5 µm which is more than its thickness (Fig. 4). Therefore, it can be deduced that in the case of the single layer coating the pin –at the last stages of wear test (after 500 m)– reaches the steel substrate, which considerably increases the COF value. The high magnification SEM image of the wear track center in Fig. 11 (a) shows the presence of holes, cracks and grooves in this region. The formation of grooves on the sample surface can be attributed to a three-body wear mechanism, due to the high hardness of the wear debris generated upon coating micro-cracking. The formation of cracks can be related to the fatigue wear of the substrate. As these cracks intersect each other, spallation of the substrate occurs, which is made evident by the holes on the worn surface. Additionally, adhesion wear between pin and substrate may also occur, resulting in the spallation of substrate and formation of deep holes. This phenomenon can be recognized from the fluctuations occurring in the curve of COF vs. sliding after 500 m. Actually, after this distance, the pin gets in contact with the substrate, and due to the higher value of the COF between two metallic surfaces (substrate and pin) compared to the metal-ceramic coating contact, there is a significant increase in the COF value. The gradual increase of COF with increasing wear distance (>500 m) is related to the increasing contact surface between pin and substrate. In Fig. 11 (c) some holes can be

observed: these holes are related to the spallation of the single layer coating from the substrate due to the relatively weak adhesion of this layer.

Considering Fig. 11 (e), it can be seen that the wear track width and depth of the graded coating is smaller than that of the single layer coating. The depth of this wear track is about 2.5 µm, i.e. a value close to the overall thickness of the coating. Consequently, it can be inferred that in the case of the graded coating, the wear pin barely reaches the substrate. According to Fig. 11 (d) and (f), grooves are formed on the worn surface, which can be attributed to a three body abrasive wear mechanism similar to the single layer coating. However, due to better adhesion of the graded coating to the substrate compared to the single layer coating, the spallation phenomenon of the coating debris does not occur, and the depth of these grooves is apparently very low. According to Fig. 10, the contact between the wear pin and the interlayer can be considered as the main reason for the increasing trend of the COF of this sample after 550 m.

Table 3 demonstrates that the volume loss caused by wear in the coating without interlayer is about 4 times larger than that of the coating with the interlayer. The higher wear track depth and width, as well as the larger wear volume observed for the single layer coating reveals a remarkable improvement of the wear behavior by introducing an interlayer at the interface between the hard coating and substrate. According to results of Rockwell C and wear tests, it can be concluded that the higher adhesion and toughness of the coating with interlayer are the main reasons for increasing the wear life since hardness and elastic modulus are nearly the same for both specimens.

4. Conclusions

In the present study, single layer and graded TiSiCN coatings were deposited by PECVD on plasma nitrided H13 steel substrate. The microscopic observations showed that the plasma

nitriding process increases the surface roughness of the substrate, thereby increasing the coating/substrate interface area. Nitrogen diffusion depth was determined as 150 μm based on the hardness profile, with a surface hardness of 1350 HV. According to GDOES results, both single layer and graded TiSiCN coatings have a similar composition. For the specimen with interlayer, the composition change at coating/substrate interface is gradual. Both TiSiCN coatings have a nanocomposite structure consisting of 10-60 nm TiCN nanocrystals embedded in an amorphous silicon carbonitride matrix. Both TiSiCN coatings show similar hardness and elastic modulus; however, based on the scratch test, the normal force for crack formation and that for delamination increased for the graded coating by 117% and 40%, respectively, compared to the single layer coating. Improvement in toughness and adhesion of the coating with interlayer led to a 75% decrease in wear volume. Hence, it is concluded that the introduction of a graded interlayer at the interface of plasma nitrided H13 steel substrate and TiSiCN coating significantly improves adhesion, toughness and wear resistance of the coating.

References

[1] H.C. Barshilia, B. Deepthi, K. Rajam, Transition metal nitride-based nanolayered multilayer coatings and nanocomposite coatings as novel superhard materials, (2010).
[2] J. Musil, Hard nanocomposite coatings: thermal stability, oxidation resistance and toughness, Surface and Coatings Technology, 207 (2012) 50-65.
[3] S. Veprek, Recent search for new superhard materials: Go nano!, Journal of Vacuum Science & Technology A: Vacuum, Surfaces, and Films, 31 (2013) 050822.
[4] I. Endler, M. Höhn, J. Schmidt, S. Scholz, M. Herrmann, M. Knaut, Ternary and quarternary TiSiN and TiSiCN nanocomposite coatings obtained by Chemical Vapor Deposition, Surface and Coatings Technology, 215 (2013) 133-140.
[5] F. Movassagh-Alanagh, A. Abdollah-zadeh, M. Aliofkhazraei, M. Abedi, Improving the wear and corrosion resistance of Ti–6Al–4V alloy by deposition of TiSiN nanocomposite coating with pulsed-DC PACVD, Wear, 390 (2017) 93-103.
[6] F. Movassagh-Alanagh, A. Abdollah-zadeh, M. Asgari, M.A. Ghaffari, Influence of Si content on the wettability and corrosion resistance of nanocomposite TiSiN films deposited by pulsed-DC PACVD, Journal of Alloys and Compounds, 739 (2018) 780-792.
[7] M. Abedi, A. Abdollah-zadeh, M. Bestetti, A. Vicenzo, A. Serafini, F. Movassagh-Alanagh, The effects of phase transformation on the structure and mechanical properties of

TiSiCN nanocomposite coatings deposited by PECVD method, Applied Surface Science, 444 (2018) 377-386.
[8] M. Dayan, M. Shengli, K. Xu, Superhard nanocomposite Ti–Si–C–N coatings prepared by pulsed-dc plasma enhanced CVD, Surface and Coatings Technology, 200 (2005) 382-386.
[9] S. Ma, D. Ma, Y. Guo, B. Xu, G. Wu, K. Xu, P.K. Chu, Synthesis and characterization of super hard, self-lubricating Ti–Si–C–N nanocomposite coatings, Acta Materialia, 55 (2007) 6350-6355.
[10] H. Xu, X. Nie, R. Wei, Tribological behavior of a TiSiCN coating tested in air and coolant, Surface and Coatings Technology, 201 (2006) 4236-4241.
[11] J. Lin, R. Wei, D.C. Bitsis, P.M. Lee, Development and evaluation of low friction TiSiCN nanocomposite coatings for piston ring applications, Surface and Coatings Technology, 298 (2016) 121-131.
[12] A. Hatem, J. Lin, R. Wei, R.D. Torres, C. Laurindo, G.B. de Souza, P. Soares, Tribocorrosion behavior of low friction TiSiCN nanocomposite coatings deposited on titanium alloy for biomedical applications, Surface and Coatings Technology, 347 (2018) 1-12.
[13] W. Li, P. Liu, Z. Xue, F. Ma, K. Zhang, X. Chen, R. Feng, P.K. Liaw, Microstructures, mechanical behavior and strengthening mechanism of TiSiCN nanocomposite films, Scientific reports, 7 (2017) 2140.
[14] J. Li, Y. Wang, Y. Yao, Y. Wang, L. Wang, Structure and tribological properties of TiSiCN coating on Ti6Al4V by arc ion plating, Thin Solid Films, 644 (2017) 115-119.
[15] K. Holmberg, A. Mathews, Coatings tribology: a concept, critical aspects and future directions, Thin Solid Films, 253 (1994) 173-178.
[16] H. Yan, J. Hua, R. Shivpuri, Flow stress of AISI H13 die steel in hard machining, Materials & design, 28 (2007) 272-277.
[17] M. Azadi, A. Sabour Rouhaghdam, S. Ahangarani, Properties of TiC coating by pulsed DC PACVD, Journal of Coatings, 2013 (2013).
[18] K. Taherkhani, F. Mahboubi, Investigation nitride layers and properties surfaces on pulsed plasma nitrided hot working steel AISI H13, Iran. J. Mater. Sci. Eng, 10 (2013) 29-36.
[19] A.A. El-Rahman, R. Wei, A comparative study of conventional magnetron sputter deposited and plasma enhanced magnetron sputter deposited Ti–Si–C–N nanocomposite coatings, Surface and Coatings Technology, 241 (2014) 74-79.
[20] C.-C. Chang, J.-G. Duh, Duplex coating technique to improve the adhesion and tribological properties of CrAlSiN nanocomposite coating, Surface and Coatings Technology, 326 (2017) 375-381.
[21] A. Voevodin, S. Walck, J. Zabinski, Architecture of multilayer nanocomposite coatings with super-hard diamond-like carbon layers for wear protection at high contact loads, Wear, 203 (1997) 516-527.
[22] F. Cemin, C. Boeira, C. Figueroa, On the understanding of the silicon-containing adhesion interlayer in DLC deposited on steel, Tribology International, 94 (2016) 464-469.
[23] S. Zhang, D. Sun, Y. Fu, H. Du, Toughening of hard nanostructural thin films: a critical review, Surface and Coatings Technology, 198 (2005) 2-8.
[24] I. Dahan, U. Admon, N. Frage, J. Sariel, M. Dariel, J. Moore, The development of a functionally graded TiC–Ti multilayer hard coating, Surface and Coatings Technology, 137 (2001) 111-115.
[25] Y. Liu, E. Meletis, Tribological behavior of DLC coatings with functionally gradient interfaces, Surface and Coatings Technology, 153 (2002) 178-183.
[26] A. Voevodin, R. Bantle, A. Matthews, Dynamic impact wear of TiCxNy and Ti-DLC composite coatings, Wear, 185 (1995) 151-157.

[27] S.P. Chuan, J.A. Ghani, S.H. Tomadi, C.H.C. Hassan, Analysis of Ti-base hard coating performance in machining process: a review, Journal of Applied Sciences(Faisalabad), 12 (2012) 1882-1890.
[28] I. Endle, E. Wolf, A. Leonhardt, V. Richter, Preparation, characterization and wear behaviour of PACVD cermets, Surface and Coatings Technology, 72 (1995) 37-42.
[29] H.O. Pierson, Handbook of chemical vapor deposition: principles, technology and applications, William Andrew1999.
[30] R.J. Shul, S.J. Pearton, Handbook of advanced plasma processing techniques, Springer Science & Business Media2011.
[31] N. Vidakis, A. Antoniadis, N. Bilalis, The VDI 3198 indentation test evaluation of a reliable qualitative control for layered compounds, Journal of Materials Processing Technology, 143 (2003) 481-485.

Tables' captions

Table 1: Parameters of plasma nitriding and deposition processes.

Table 2: Mechanical properties of TiSiCN coatings with and without the graded interlayer

Table 3: Wear area and wear volume obtained from the ball-on-disk test.

Table

Table 1.

	T (C^0)	f (kHz)	U (V)	P (torr)	Ar (sccm)	H_2 (sccm)	N_2 (sccm)	CH_4 (sccm)	$TiCl_4$ (sccm)	$SiCl_4$ (sccm)	Surface roughenss R_a (µm)
PN	500	10	650	1	75	75	40	-	-	-	0.130
Batch 1	500	12	650	0.2	100	200	30	10	5	1	0.045
Batch 2	500	12	650	0.2	100	200	0-30	0-10	5	1	0.062

Table 2.

Type of TiSiCN coating	**Hardness (GPa)**	**Elastic modulus (GPa)**	**L_{c1} (N)**	**L_{c2} (N)**
Single layer	39±3	335±21	0.6±0.2	2.7±0.3
With graded interlayer	41±4	341±23	1.3±0.2	3.8±0.4

Table 3.

Sample	Wear Area (μm^2)	Wear Volume (μm^3)
TiSiCN	1934	121516
Functionally graded TiSiCN	599	37636

Figures' captions

Fig. 1: A schematic diagram of the typical structure of TiSiCN coatings: (a) without the interlayer, (b) with the graded interlayer.

Fig. 2: SEM micrograph showing the surface of H13 steel substrate after plasma nitriding process.

Fig. 3: Hardness depth profile through the thickness of the nitrided layer.

Fig. 4: SEM cross-sectional images of (a) single layer and (b) graded TiSiCN coatings.

Fig. 5: GDOES depth profiling analysis of TiSiCN coatings deposited without (a) and with (b) graded interlayer.

Fig. 6: TEM micrographs and, in the insets, SAED patterns of (a) single layer and (b) graded TiSiCN coatings.

Fig. 7: Diagrams of COF, intensity of acoustic emission and OM images of wear tracks on (a) single layer and (b) graded TiSiCN coatings.

Fig. 8: The fracture surface of sliding tracks on (a) single layer and (b) graded TiSiCN coatings.

Fig. 9: OM image of indentation made by Rockwell C indenter on (a) single layer and (b) graded TiSiCN coatings.

Fig. 10: (a), (b) and (c) SEM and surface profilometry images of single layer TiSiCN coating and (d), (e) and (f) SEM and surface profilometry images of graded TiSiCN coating.

Figure

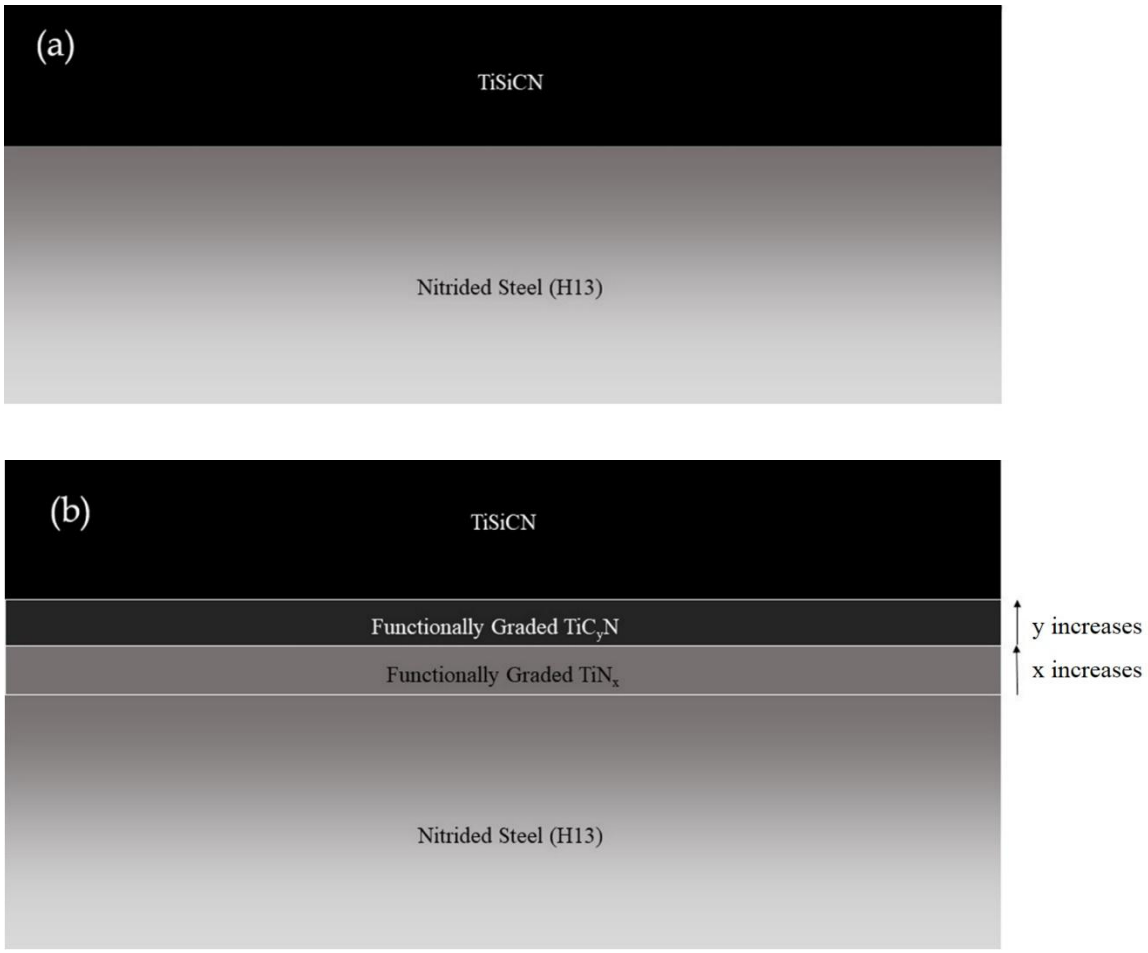
(a)
TiSiCN
Nitrided Steel (H13)
(b)
TiSiCN
Functionally Graded TiC_yN
Functionally Graded TiN_x
Nitrided Steel (H13)
y increases
x increases

Fig. 1.

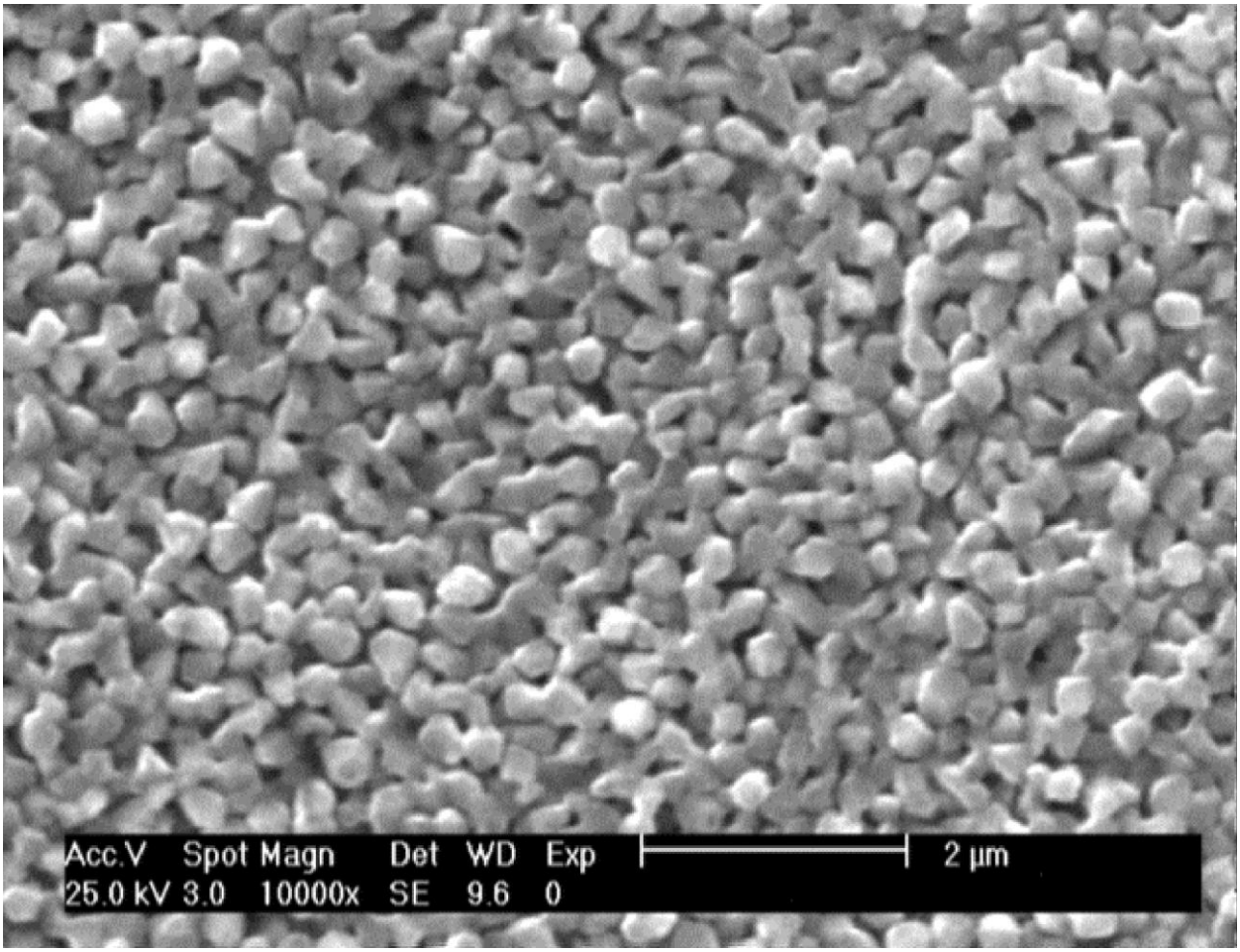

Fig. 2.

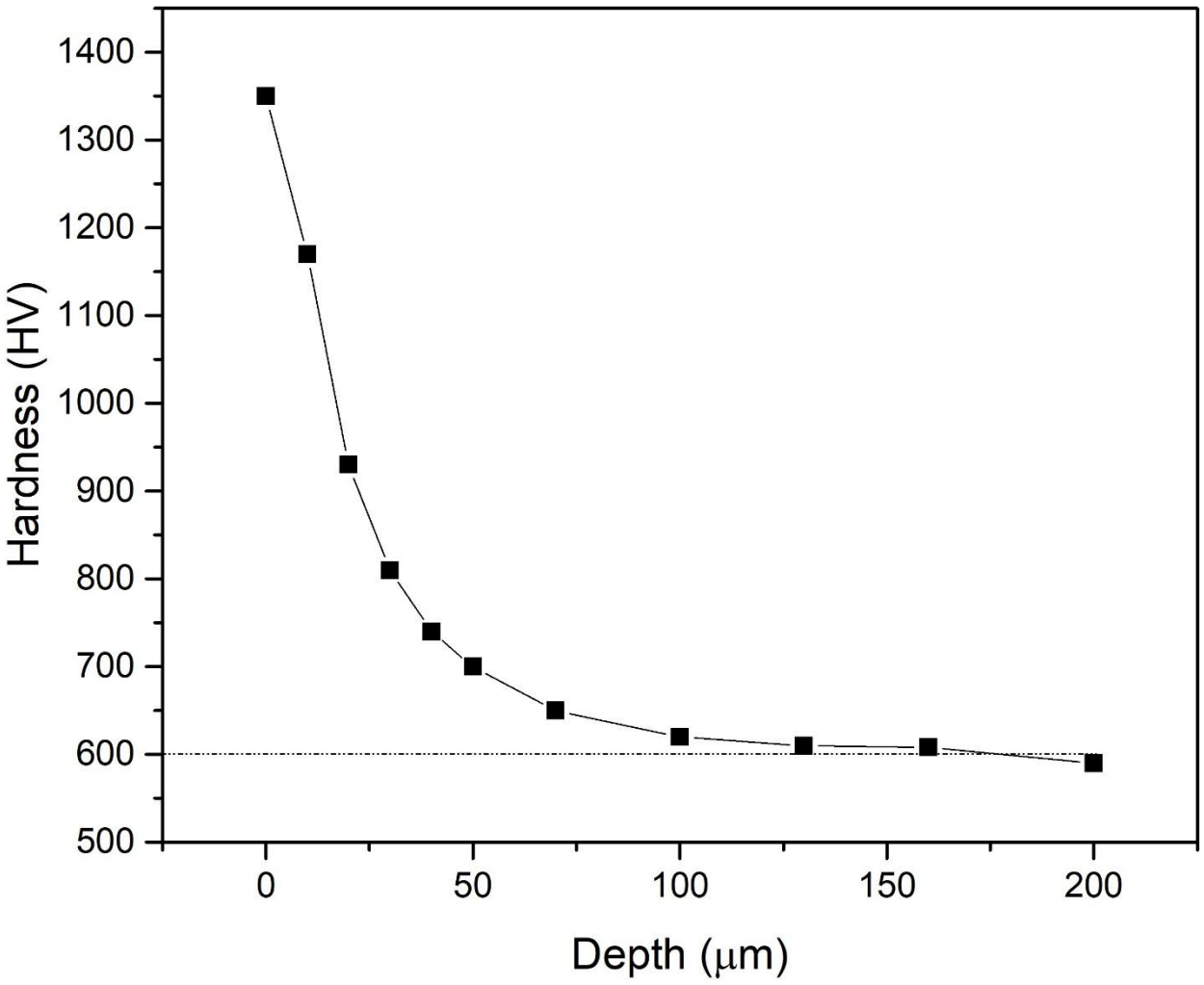
Hardness (HV)
1400
1300
1200
1100
1000
900
800
700
600
500
0
50
100
150
200
Depth (μm)

Fig. 3.

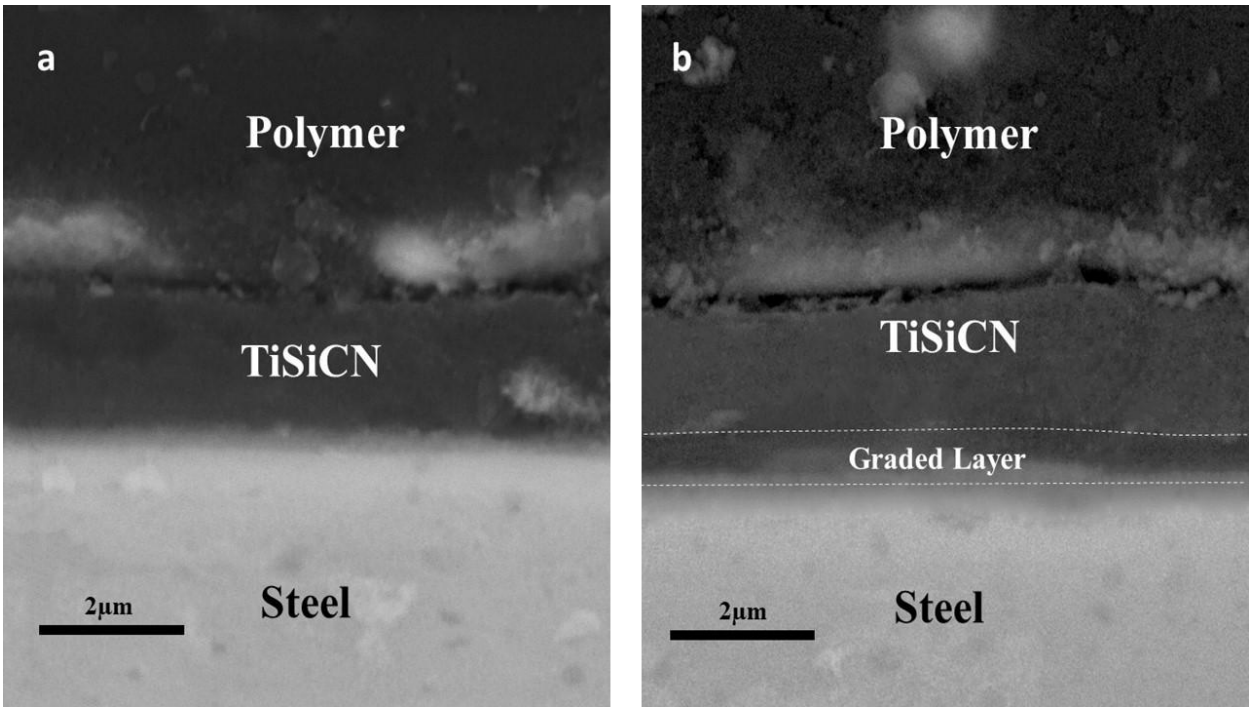
a
Polymer
TiSiCN
2µm
Steel
b
Polymer
TiSiCN
Graded Layer
2µm
Steel

Fig. 4.

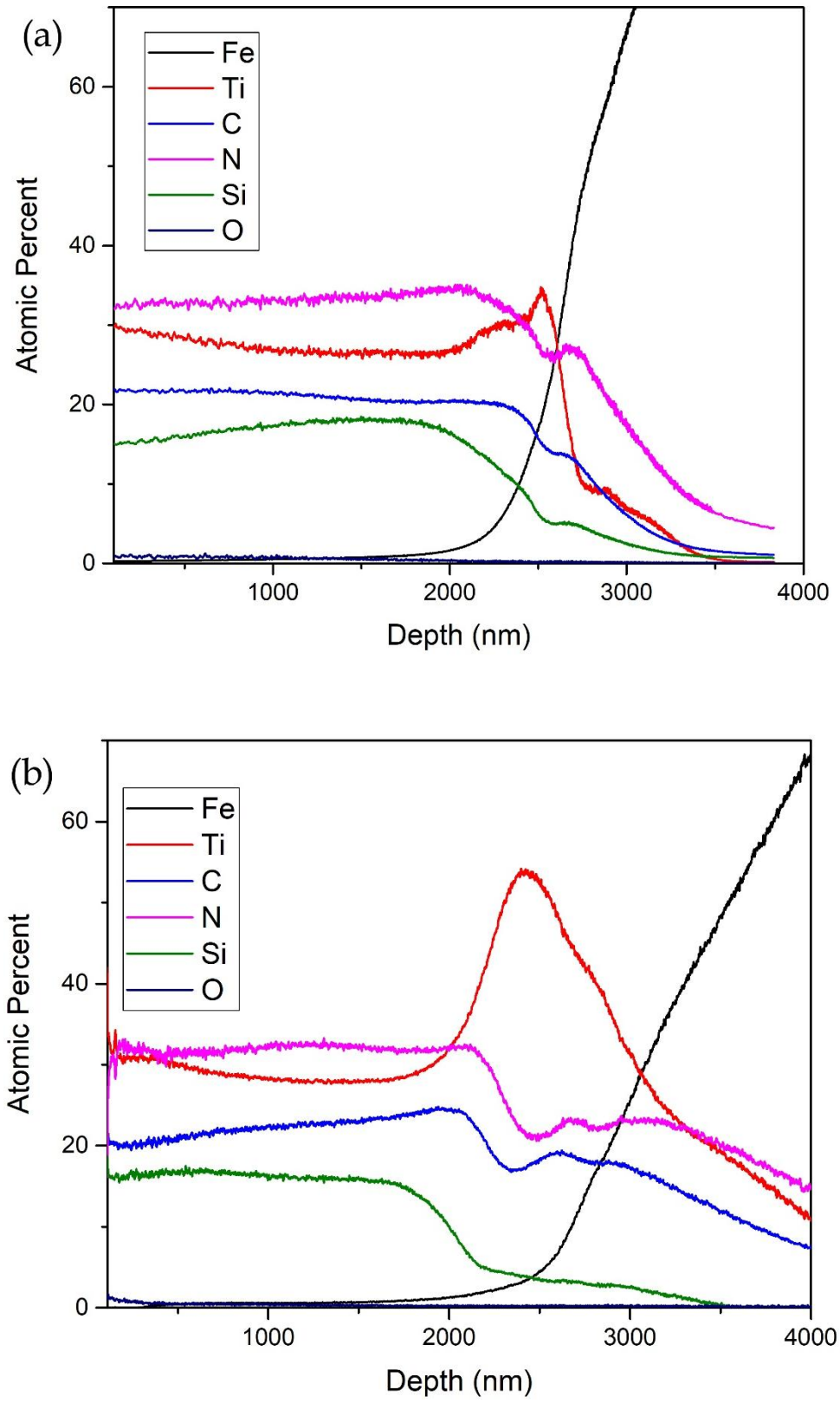
(a)
Fe
Ti
C
N
Si
O
Atomic Percent
0
20
40
60
1000
2000
3000
4000
Depth (nm)
(b)
Fe
Ti
C
N
Si
O
Atomic Percent
0
20
40
60
1000
2000
3000
4000
Depth (nm)

Fig. 5.

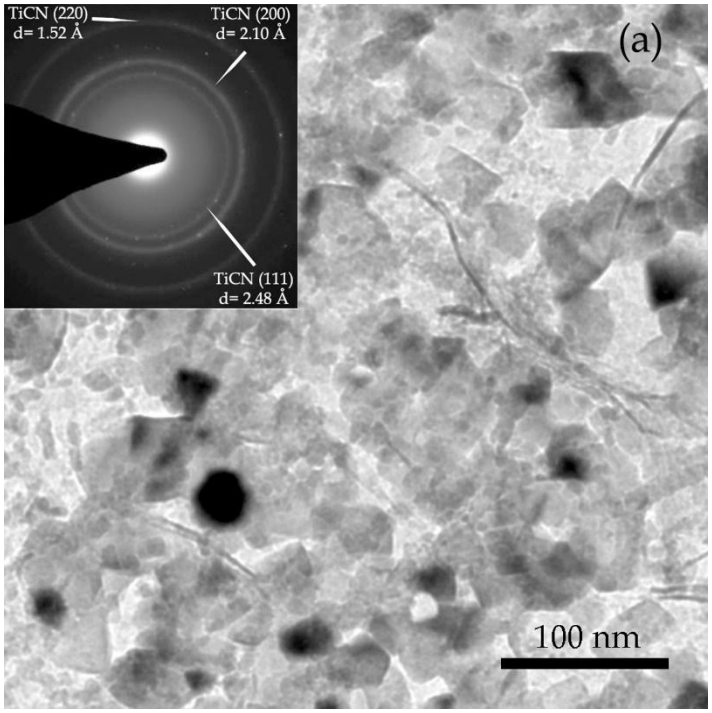
TiCN (220)
d= 1.52 Å
TiCN (200)
d= 2.10 Å
TiCN (111)
d= 2.48 Å
(a)
100 nm

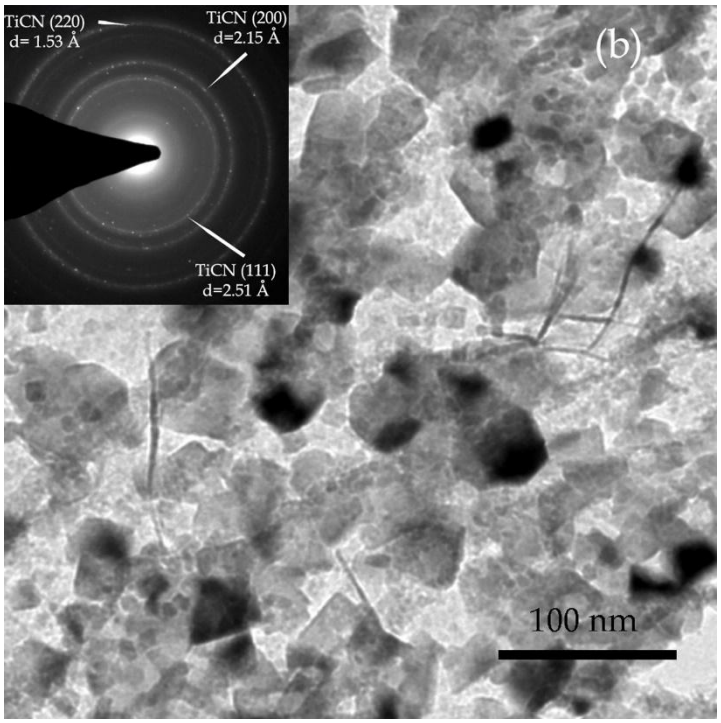
TiCN (220)
d= 1.53 Å
TiCN (200)
d=2.15 Å
TiCN (111)
d=2.51 Å
(b)
100 nm

Fig. 6.

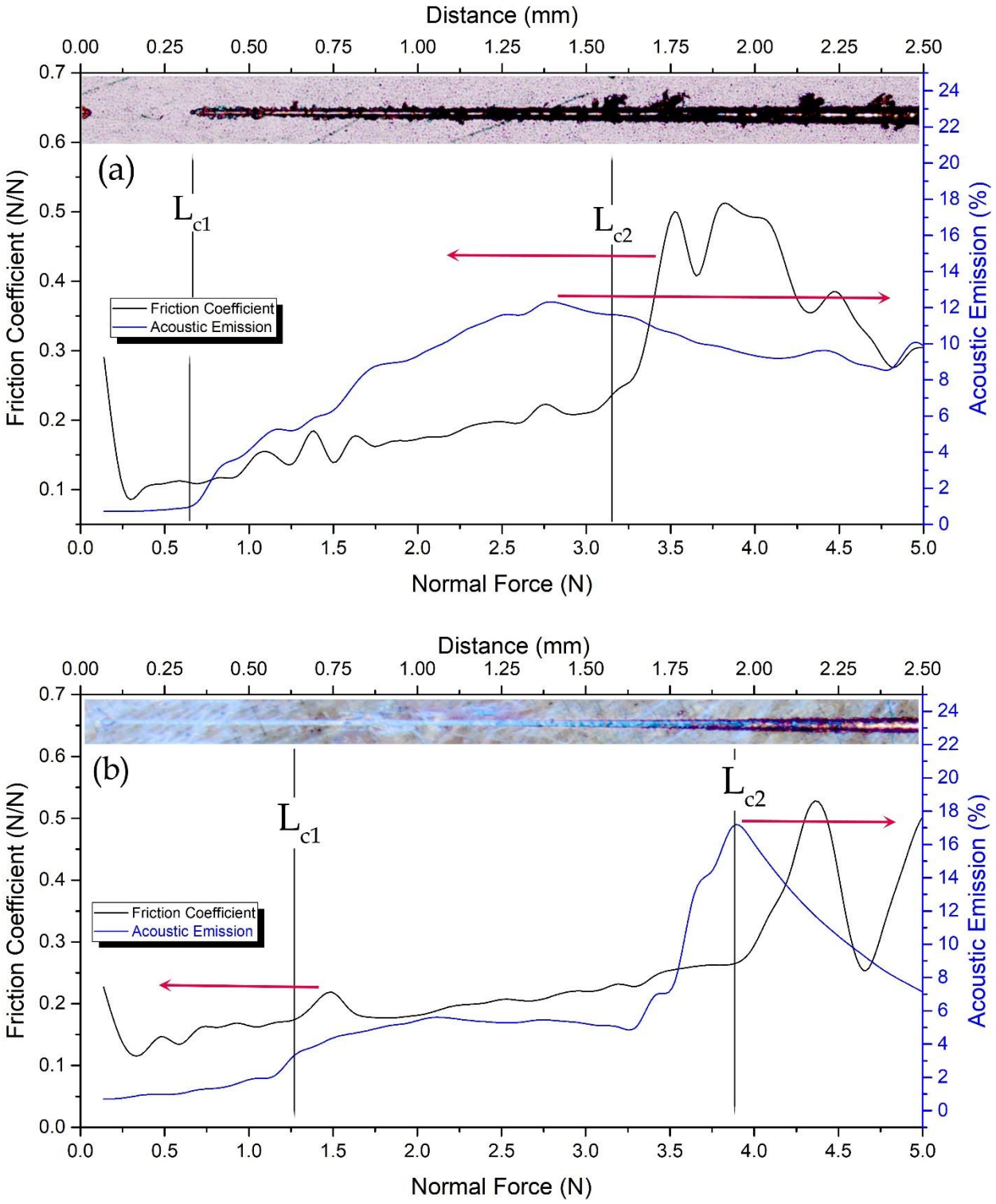
Distance (mm)
0.00 0.25 0.50 0.75 1.00 1.25 1.50 1.75 2.00 2.25 2.50
(a)
L_{c1}
L_{c2}
Friction Coefficient
Acoustic Emission
Friction Coefficient (N/N)
Acoustic Emission (%)
Normal Force (N)
0.0 0.5 1.0 1.5 2.0 2.5 3.0 3.5 4.0 4.5 5.0
(b)
L_{c1}
L_{c2}
Friction Coefficient
Acoustic Emission
Friction Coefficient (N/N)
Acoustic Emission (%)
Normal Force (N)

Fig. 7.

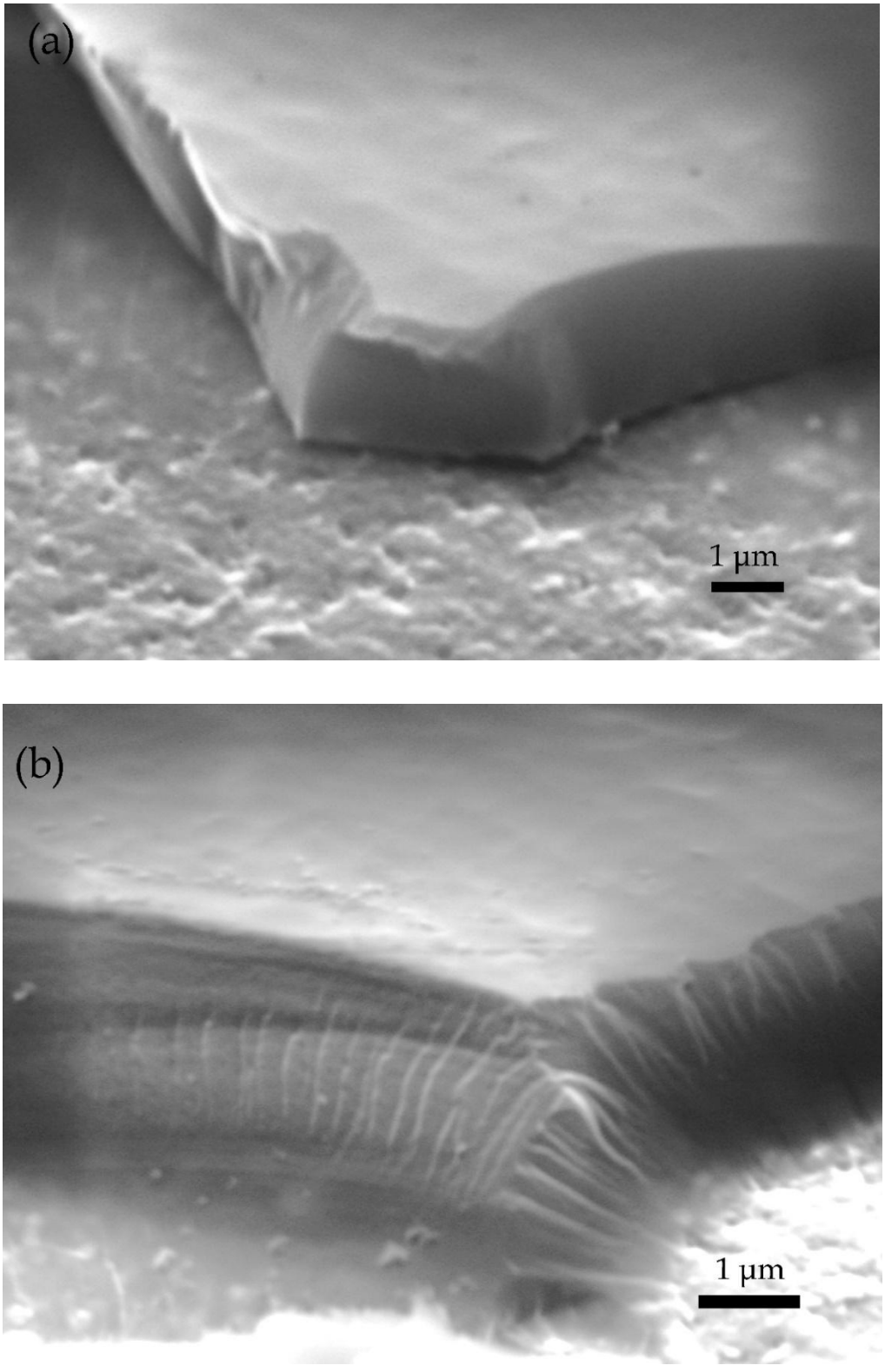

Fig. 8.

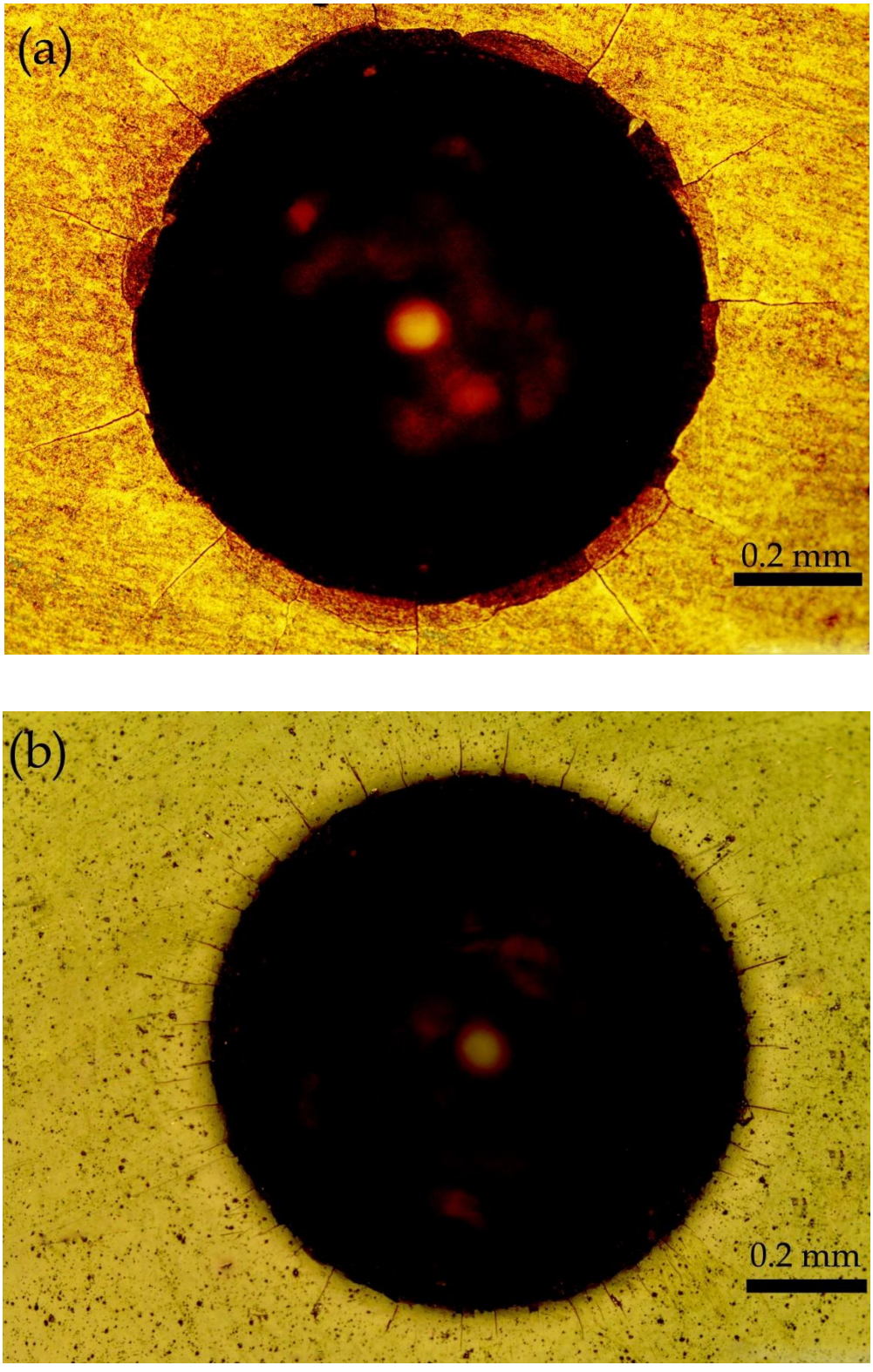

Fig. 9.

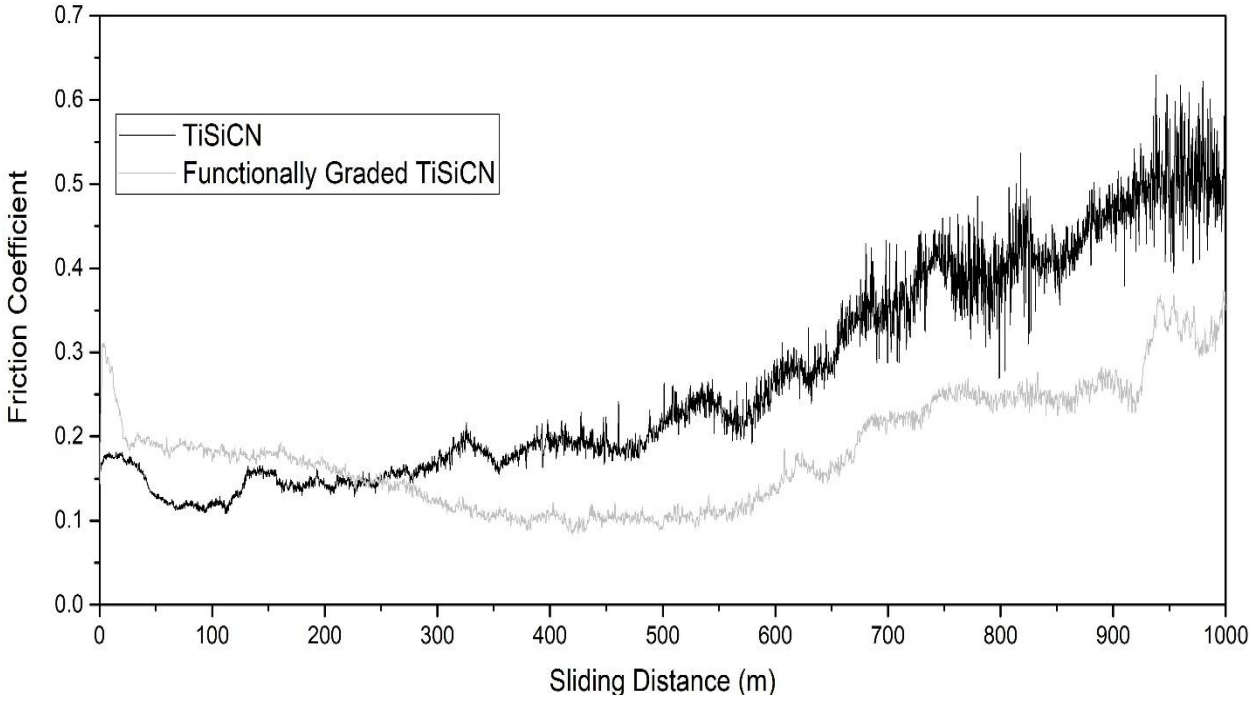
TiSiCN
Functionally Graded TiSiCN
Friction Coefficient
Sliding Distance (m)
0.0
0.1
0.2
0.3
0.4
0.5
0.6
0.7
0
100
200
300
400
500
600
700
800
900
1000

Fig. 10.

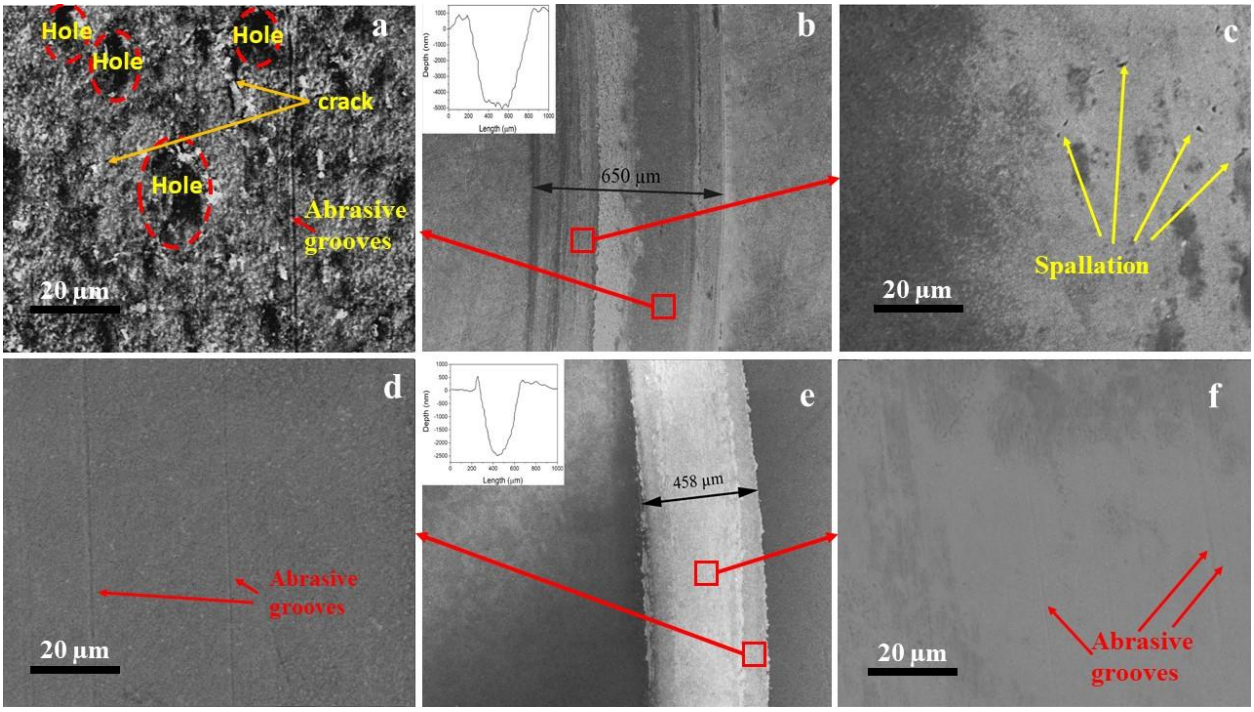
a
Hole
Hole
Hole
crack
Hole
Abrasive
grooves
20 µm
b
650 µm
c
Spallation
20 µm
d
Abrasive
grooves
20 µm
e
458 µm
f
20 µm
Abrasive
grooves

Fig. 11.